The structures of the precursor $Hf(O^nBu)_4$ and its modification in solution: EXAFS-investigation in combination with XANES- and IR-spectroscopy†

Matthias Bauer,*[a] Sonja Müller,[a] Guido Kickelbick[b] and Helmut Bertagnolli[a]

Received (in Montpellier, France) 10th May 2007, Accepted 10th July 2007
First published as an Advance Article on the web 27th July 2007
DOI: 10.1039/b707079a

The solution structure of hafnium-*n*-butoxide $Hf(O^nBu)_4$, an important precursor for the sol–gel preparation of hafnium oxide containing materials, was studied in solution in pure toluene, and in presence of acetylacetone, *iso*-propanol and tetrahydrofuran by EXAFS-, XANES- and IR-spectroscopy. The combination of these three methods and the additional measurements and discussions of well known solid state references allow us to identify structural motives and to gain a detailed picture of the structures formed in solution without any *a priori* knowledge about these structures. The dimeric structure of crystalline $Hf(O^nBu)_4$ is not preserved in solution and a trimeric cyclic structure is formed. While the addition of HO^iPr and THF does not induce any change of the formed complexes, one equivalent of Hacac reduces the degree of aggregation by the partial formation of dimers. In the presence of two and three equivalents of Hacac, solely monomeric species are formed. The obtained structural parameters are used to establish for the first time an empirical correlation of a spectral feature in the XANES region with the average oxygen coordination number.

Introduction

The sol–gel process[1] has been extensively studied as a route to high-purity oxides,[2] thin-film coatings,[3] fibres,[4] multicomponent ceramics[5] or new binary oxides and hybrid materials.[6] Key steps in this process are hydrolysis and condensation reactions of molecular precursors, such as alkoxides.[7] Metal alkoxides generally form aggregated compounds in solution, and the degree of aggregation and the chemical constitution of the used molecular precursors are important parameters that influence the relative reaction rates of the condensation reaction. Oligomers of the type $[M(OR)_n]_x \cdot y$ HOR are often used as precursors for the sol–gel preparation of materials. The oligomerization degree itself is influenced by the competition between chelating ligands and bridging alkoxide groups or by addition of more bulky Lewis bases like *iso*-propanol HO^iPr or cyclic ethers, for example THF. Thus the structure of the alkoxide precursors and their modification by various coordinating groups, which are different from the alkoxide group, are of special interest for the preparation of tailor made materials. Their reaction rates can be influenced by addition of chelating ligands like acetylacetone Hacac (2,4-pentadione), which reduce the possibility of nucleophilic attack by H_2O through blocking coordination sites of the metal ion.

In general, alkoxides of transition metals tend to saturate their coordination sites in non-polar solvents by alkoxide bridging, while in polar solvents the association of solvent molecules is favoured.[8–10] In the solid state the structure of different metal alkoxides was determined by the analyses of single crystals by X-ray diffraction.[11,12] But whether the molecular structures found in solid state references are similar to those found in solution is often questionable.[13]

Classical methods to determine the molecular complexity of metal alkoxides like ebullioscopic or cryoscopic measurements suffer from unstable reproducibility and large errors.[8] Mass spectrometry is a method often applied, but has the disadvantage of not directly probing the formed structures *in situ*.[9] Various other spectroscopic methods (Raman-, IR-, ^{1}H-NMR-, multinuclear NMR-spectroscopy) were applied to identify the molecular structures of alkoxides in solution.[14] However, these methods do not provide direct information on the local structure of the central metal atom in contrast to X-ray absorption spectroscopy that probes the local environment of a metal atom directly. Only a few X-ray absorption (XAS) experiments on solutions of alkoxides are known from the literature, *e.g.* titanium[15] and zirconium,[10] mixed titanium–zirconium[16] and cerium alkoxides.[17] In the case of hafnium alkoxides, to the best of our knowledge no XAS investigations have yet been carried out. The present studies could further enlighten the structures formed in solution, since NMR-investigations were unable to identify the species formed after dissolving and modifying well-characterized solid Hf-alkoxides.[14d] Only for aqueous solutions of hafnium salts has the important EXAFS technique been applied so far,[18,19]

[a] *Institute of Physical Chemistry, University of Stuttgart, Pfaffenwaldring 55, 70569 Stuttgart, Germany. E-mail: m.bauer@ipc.uni-stuttgart.de; Fax: +49 711 685 64443; Tel: +49 711 685 64472*
[b] *Institute of Materials Chemistry, Technical University Vienna, Getreidemarkt 9-165, 1060 Vienna, Austria. E-mail: kickelgu@mail.zserv.tuwien.ac.at; Fax: +43 1 58801 15399; Tel: +43 1 58801 15321*

† Electronic supplementary information (ESI) available: Fig. SF1–SF4 and experimental details. See DOI: 10.1039/b707079a

but the results of these studies are of limited value for solutions of Hf alkoxides in anhydrous, aprotic solvents.

Therefore, we wanted to extend these studies and apply XAFS spectroscopy to Hf-precursors used for the sol–gel process. We chose $Hf(O^nBu)_4$ (**1**) in toluene (**2**) as a model system for this purpose. Since we also wanted to show the importance of XAFS spectroscopy for chemical analyses of solution structures, about which usually no prior knowledge exists, we restricted ourselves to the interpretation of the radial distribution functions instead of multiple scattering calculations. With this approach in combination with XANES- and IR-spectroscopy, it was possible to identify the species formed by **1** in **2**.

In the first part of this work, the structures of solid state references, relevant for the discussion of the experimental results, will be briefly reviewed. The effects of the Lewis bases THF (tetrahydrofuran) and HO^iPr (*iso*-propanol, 2-propanol), and of the chelating compound Hacac (acetylacetone, 2,4-pentadione) on the structure formed by **1** in **2** are studied in the third part. Finally, the results of the EXAFS analyses are correlated to a particular XANES-feature at around 9.58 keV. Throughout the whole work, the behaviour of $Hf(O^nBu)_4$ is compared to that of the homologous $Zr(O^nBu)_4$,[20] since despite the generally very similar chemical behaviour of zirconium and hafnium, the alkoxides of both metals can show significant differences.[21]

Experimental

Samples

Hafnium-*n*-butoxide (95% in *n*-butanol) was purchased from ABCR and used as obtained without further purification. The concentration of hafnium in toluene in all measurements was 0.18 mol l^{-1} to achieve an optimal transmission signal in the EXAFS measurement. Sample handling and addition of the dry and purified complexing agents THF, HO^iPr and Hacac were carried out under argon atmosphere. After adding the donor compounds, each solution was allowed to equilibrate for two hours under stirring at room temperature in order to ensure equivalent conditions during the measurements. Monoclinic HfO_2 was purchased form Sigma–Aldrich and used as received.

IR-spectroscopic measurements

FT-IR spectra were recorded using a Bruker IFS FT-infrared spectrometer. The measurements were carried out in ATR mode utilizing a silicon crystal. All the spectra were collected in the region from 5000 to 400 cm^{-1} with a resolution of 2 cm^{-1}. 8000 scans were accumulated and averaged for each spectrum. As no spectral changes were observed even 24 h after the addition of up to four equivalents Hacac, the stability of the formed structures was proved.

EXAFS measurements

The EXAFS measurements were performed at beamline A1 of the Hamburger Synchrotronstrahlungslabor (HASYLAB) at DESY (Hamburg, Germany). For the Hf L_{III}-edge (9.561 keV) a Si(111) channel-cut double crystal monochromator was used. The synchrotron beam current at HASYLAB (positron energy 4.45 GeV) was between 80–140 mA. The experiments were carried out under ambient conditions at 20 °C. Energy resolution was estimated to be about 1 eV for the Hf L_{III}-edge. All the spectra were collected in transmission mode with ion chambers filled with argon. A sealed liquid sample cell for handling of air sensitive samples[22] was used in the EXAFS experiment to prevent hydrolysis. The path length for the samples of **1** was 6 mm in order to achieve an edge jump of approximately 1.5.

Data analysis

Data evaluation started with background removal from the experimental absorption spectrum by subtraction of a Victoreen-type polynomial. Then the background subtracted spectrum was convoluted with a series of Gauss functions of increasing FWHM and the common intersection point of the convoluted spectra was taken as energy E_0.[23] To determine the smooth part of the spectrum, corrected for pre-edge absorption, a piecewise polynomial was used. It was adjusted in such a way that the low-R components of the resulting Fourier transform were minimal. After division of the background subtracted spectrum by its smooth part, the photon energy was converted to photoelectron wave numbers k. The resulting EXAFS functions presented in this work were weighted with k^3 after background removal and conversion into k-space. Data analysis was performed in k-space according to the curved wave formalism of the program EXCURV98,[24] which carries out calculations of the EXAFS function according to a formulation in terms of radial distribution functions:

$$\chi(k) = \sum_j S_0^2(k) F_j(k) \int P_j(r_j) \frac{e^{-2r_j/\lambda}}{kr_j^2} \sin[2kr_j + \delta_j(k)]\, \mathrm{d}r_j$$

This method is suitable especially for chemical analyses of amorphous systems and solutions, since in contrast to path-by-path evaluation methods[25] it does not require detailed structural information as input and results in a model independent description of the system. No Fourier filtering was applied, since the spectra show a high signal-to-noise ratio. In course of the fitting procedure, the overall amplitude reduction factor S_0^2 (k) was kept constant at a value of 0.8, which was determined for the HfO_2 reference. To minimize the risk of misinterpretations and to achieve a reliable determination of the coordination numbers, consistency of the k^3-weighted with k^2- and k^1-weighting schemes was checked. Differences in the obtained coordination numbers were within the error bar. XALPHA phase and amplitude functions[24] were used to calculate the theoretical spectra and the mean free path of the scattered electrons was calculated from the imaginary part of the potential (VPI was set to −4.00). An inner potential correction E_f was introduced to account for phase differences of the experimental and theoretical EXAFS functions.

The quality of the least-square fit is reflected in the R-factor, calculated according to

$$R = \frac{\sum |\chi^{\mathrm{theo}} - \chi^{\mathrm{exp}}| k^3 \mathrm{d}k}{\sum |\chi^{\mathrm{exp}}| k^3 \mathrm{d}k} \cdot 100\%$$

To avoid overinterpretation by fitting too many parameters to the experiment, the number of independent points was calculated by $N_{ind} = 2\pi^{-1}(\Delta k \Delta R)$,[24b] where Δk is the range in k-space used for the analysis and ΔR the range in which distances are fitted. To account for the non-ideal signal packing this number was multiplied by 2/3 to achieve a reasonable number of free fitting parameters N_{free}. The accuracy of the determined coordination numbers is 10%, of the distances 1%, and again 10% for the Debye–Waller factor σ^2.[26]

Evaluation and least square fit of the XANES region were carried out by using the WINXAS program package.[27] To obtain a good fit, an arctan step function representing the transition of the ejected photoelectron to the continuum in combination with an asymmetric pseudo-Voigt function was used. In the latter, the percentages of the Gaussian and Lorentzian part were iterated to reproduce the experimental white line properly. Although applying this very flexible function, by which spectral information contained in the white-line can not be resolved any further, this procedure is justified by the fact, that the subject of this work is the signal after the white line. Also, the number of parameters in the fits is minimized in this way. To reproduce the experimental signal at 9.58 keV, an asymmetric Gaussian function was used for all samples. No constraints were used in the least square fit and several sets of initial parameters were applied, which gave all identical reproducible results.

Results and discussions

Structures of solid state references

As mentioned in the introduction, almost no structural information is available for hafnium alkoxides in solutions in non-aqueous liquids. Transition metal alkoxides often show an oligomerization in solution and in crystal structure to complete their coordination environment. This is usually done by two mechanisms, the use of alkoxide bridges between different metal centers and the coordination of free alcohols. A key role in the degree of oligomerization and the complexity of the structures is played by the sterical demand of the ligands: as a rule of thumb, smaller alkoxides such as ethoxides favor large multinuclear structures, while sterically more demanding alkoxides such as isopropoxides favor low degrees of oligomerization. If the alkoxides are substituted by bidentate or multidentate ligands the degree of oligomerization is usually reduced because more coordination sites at the metal center are occupied compared to the monodentate alkoxide ligands. In order to obtain an impression of which structures and which oligomeric species of hafnium alkoxides exist, a brief review of crystalline references relevant for the formation of clusters is discussed in the following section. The corresponding averaged values of coordination numbers and distances, as they would be obtained by EXAFS spectroscopy, are summarized in Table 1.

The dimer $Hf_2(O^iPr)_8(HO^iPr)_2$ (**3**) consists of edge sharing octahedra with one hafnium backscatterer at a distance of 3.47 Å and each hafnium center coordinated by two equatorial terminal $[O^iPr]^-$ ligands at 1.93 Å. The second oxygen shell is constituted by one axial $[O^iPr]^-$, one axial HO^iPr and two bridging $[O^iPr]^-$ ligands at an average distance of 2.16 Å for the four O-atoms. Since almost all systems, discussed here, exhibit two oxygen shells, the first shell is denoted as O1 and the second one as O2 in Table 1. The structure of $Hf(O^iPr)_4(HO^iPr)$ is similar to the solid $Zr(O^iPr)_4(HO^iPr)_4$ analog.[28]

The hexamer $Hf_6O_2(OEt)_{20}(EtOH)_2$ (**4**)[29] shows an average Hf coordination number of 2.7 at a distance of 3.45 Å and an octahedral oxygen coordination, with average distances of

Table 1 Structural parameters of solid state references as they would be determined by EXAFS spectroscopy[a]

Reference	Oligomerization	Structure	N(O1) R(O1)	N(O2) R(O2)	N(Hf) R(Hf)	Deduced model structure
3: $Hf_2(O^iPr)_8(HO^iPr)_2$ [11]	Dimer	Linear	2 1.93 Å	4 2.16 Å	1 3.47 Å	**I**
4: $Hf_6O_2(OEt)_{20}(EtOH)_2$ [29]	Hexamer	Chair	2.3 1.97 Å	3.7 2.13 Å	2.7 3.45 Å	—
5: $Hf_3O(OEt)_{10}$ [29,b]	Trimer	Triangle	2 1.97 Å	4 2.13 Å	2 3.45 Å	**II**/**IV**[c]
6: $Hf_4O_2(OMc)_{12}$ [21]	Tetramer	Rectangle	1.5 2.06 Å	6 2.18 Å	2.5 3.54 Å	**III**
7: $Hf_2(O^iPr)_6(tmhd)_2$ [30]	Dimer	Linear	2 1.94 Å	4 2.15 Å	1 3.48 Å	**V**[c]
8: $Hf_2(O^nPr)_6(tmhd)_2$ [14d]	Dimer	Linear	2 1.90 Å	4 2.12 Å	1 3.46 Å	**V**[c]
9: $Hf_2(O^iPr)_2(tmhd)_4(OH)_2$ [14d]	Dimer	Linear	1 1.89 Å	6 2.14 Å	1 3.56 Å	**VII**[c]
10: $Hf(O^tBu)_2(mmp)_2$ [3a]	Monomer	—	2 1.93 Å	4 2.18 Å	—	**VI**[c]
11: $Hf(O^iPr)(tmhd)_3$ [14d]	Monomer	—	1 1.81 Å	6 2.13 Å	—	**VIII**[c]
12: $Hf(acac)_4$ [31]	Monomer	—	—	8 2.20 Å	—	—

[a] Not identical with, but deduced from crystallographic data. [b] Values are deduced from the corresponding hafnium sub-framework and oxygen shells of **4** and $Zr_3O(O^tBu)_{10}$. [c] The reference compounds serve as model for the hafnium framework, and some changes to the oxygen coordination of the references were applied to obtain the deduced model structures in order to mirror the experimental data, *e.g.* the coordination of an additional neutral ROH ligand.

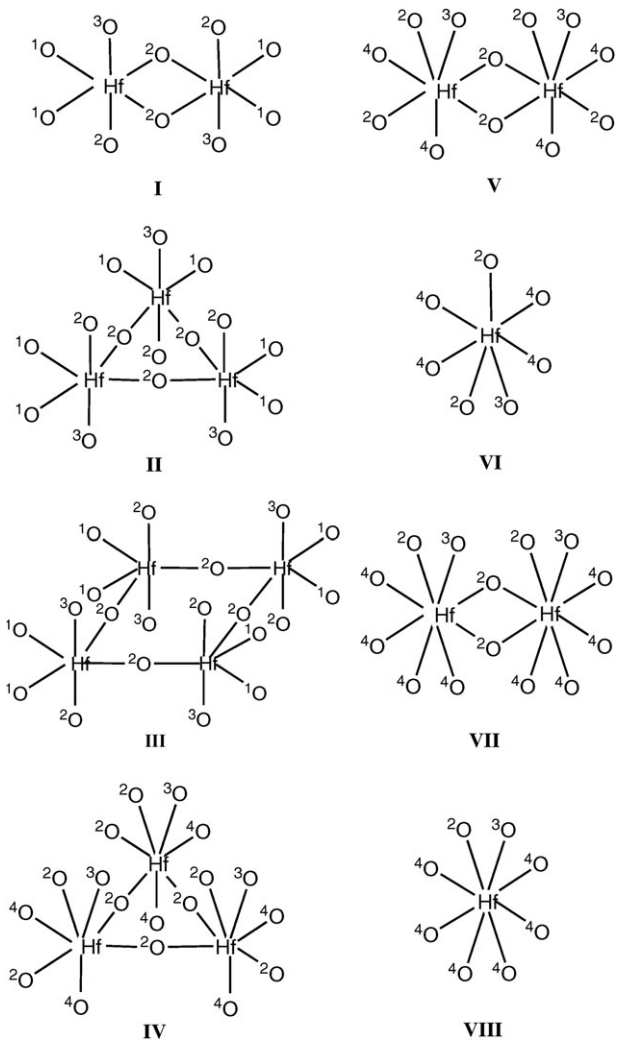

Scheme 1 Structural models used for the discussion of the EXAFS results. The nomenclature of the oxygen atoms is given in Table 2.

1.97 Å for 2.3 terminal alkoxide and 2.13 Å for 3.7 bridging ligands. In solutions, the degradation of the hexamer $Hf_6O_2(OEt)_{20}(EtOH)_2$ to trimers similar to $Zr_3O(O^tBu)_{10}$ is assumed.[29] The trimeric $Zr_3O(O^tBu)_{10}$ shows two terminal and four bridging ligands. From the structural parameters of hexameric **4** and trimeric $Zr_3O(O^tBu)_{10}$, the values that would be obtained by EXAFS measurements of the trimer $Hf_3O(OEt)_{10}$ (**5**) can be deduced, since the ionic radii of Zr^{4+} and Hf^{4+} are very similar. They are given in Table 1.

A tetrameric rectangular arrangement forms the frame of the oxocluster $Hf_4O_2(OMc)_{12}$ (OMc = methacrylate) (**6**).[21] The two different coordination sites with a mean oxygen coordination of 1.5 atoms at 2.06 Å, and six at 2.18 Å, respectively, can be averaged to one shell with an oxygen coordination number of 7.5 at 2.16 Å and the two different Hf–Hf distances, present in **6**, can be averaged to one shell with 2.5 Hf backscatterers at 3.54 Å. The complexes $[Hf_4(OH)_8(OH_2)_{16}]Cl_8$ and $[Hf_4(OH)_8(OH_2)_{16}](ClO_4)_8$, found in aqueous solutions, exhibit similar Hf–Hf distances.[18] No tetrameric structure with 6-fold coordinated hafnium centers was found in the literature.

From structure **3** the dimeric $Hf_2(O^iPr)_6(tmhd)_2$ (**7**) (tmhd = 2,2,6,6-tetramethylheptane-3,5-dionate) and $Hf_2(O^nPr)_6(tmhd)_2$ (**8**) are derived by exchange of two axial alkoxide and alcohol ligands by two bidentate $[tmhd]^-$. Therefore the structural values do not change significantly.[29] But it should be mentioned that NMR studies of both diketone-monosubstituted alkoxides in solution indicate ligand-isomerization.[14d,30]

A structure significantly different from the so far discussed dimeric species shows $Hf_2(O^iPr)_2(tmhd)_4(OH)_4$ (**9**).[14d] The sevenfold oxygen coordination in this complex is constituted by one O-atom at 1.89 Å and six at 2.14 Å. The hafnium neighbour is found at 3.56 Å.

Typical representatives of monomeric species are $Hf(O^tBu)_2(mmp)_2$ (**10**) (mmp = 1-methoxy-2-methyl-2-propanolate) with a six-fold O-coordination, seven-fold O-coordinated $Hf(O^iPr)(tmhd)_3$ (**11**) with one apical *iso*-propoxide ligand and six oxygen from tmhd (denoted in the following as equatorial) and eightfold O-coordinated $Hf(acac)_4$ (**12**), $Hf(tmhd)_4$ and $Hf(tod)_4$ with four bidentate ligands like Hacac or tod (2,7,7-trimethyl-3,5-octandione).[14d,31]

The presented references are used to deduce models that are relevant for the interpretation of the EXAFS results. The characteristic features of the different species are presented in Scheme 1 with the nomenclatures given in Table 1 (for the cluster type) and Table 2 (for the different Hf–O bonds).

It is obvious from this discussion that the important parameter for the identification of the different species in solution is the Hf–Hf coordination number, whereas the Hf–O coordination number can only be interpreted under consideration of stoichiometry and IR-spectroscopic results.

Pure $Hf(O^nBu)_4$ in toluene

Fig. 1 shows the experimental EXAFS functions $k^3 \cdot \chi(k)$ and the corresponding Fourier transforms of pure $Hf(O^nBu)_4$ (**1**) in toluene (**2**) without and with HO^iPr or THF. For completeness, spectra of the reference samples monoclinic HfO_2 [32] and $Hf_4O_2(OMc)_{12}$ (**6**)[21] are also shown in Fig. 1 and 4. Structural parameters, obtained by fitting the experimental EXAFS function of these references and **1** in **2** are given in Table 3.

Table 2 Overview of the different Hf–O bond types, together with their labelling in Scheme 1

Type of bond	Coordination/binding site	Label in Scheme 1	Bond type
Hf–OR	Octahedral/equatorial	^{1}O	O1 (~1.95 Å)
Hf–OR	7-fold/apical	^{1}O	O1 (~1.95 Å)
Hf–OR	Octahedral/axial, μ_2-bridging	^{2}O	O2 (~2.15 Å)
Hf–OR	7-fold, 8-fold/equatorial, μ_2-bridging	^{2}O	O2 (~2.15 Å)
Hf–OR	8-fold/all	^{2}O	O2 (~2.15 Å)
Hf–HOR	Octahedral, 7-fold, 8-fold/all	^{3}O	O2 (~2.15 Å)
Hf–Oacac	Octahedral, 7-fold, 8-fold/all	^{4}O	O2 (~2.15 Å)

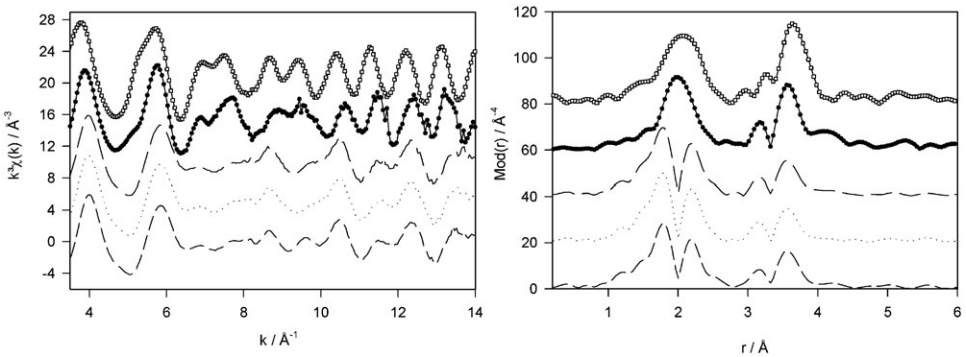

Fig. 1 Experimental $k^3 \cdot \chi(k)$ functions (left) of $Hf(OBu)_4$ (**1**) in toluene (**2**) (short dashed line), as well as containing three equivalents of HO^{i}Pr (dotted line) or THF (medium dashed line), monoclinic HfO_2 (filled circles) and $Hf_4O_2(OMc)_{12}$ (open squares) together with their Fourier transforms (right).

Table 3 Structural parameters, obtained by fitting the k^3 $\chi(k)$ weighted spectra of $Hf(OBu)_4$ (**1**) in toluene (**2**), and containing one to three equivalents of HO^{i}Pr, THF and Hacaca. For comparison the values of monoclinic HfO_2 and $Hf_4O_2(OMc)_{12}$ are also listed

Sample	Abs-Bs[b]	N(Bs)	R/Å	σÅ	Δk/Å^{-1} ΔR/Å	N_{ind} N_{free} $N_{iterated}$	E_f/eV Fit index
$Hf(OBu)_4$	Hf–O1	1.9 ± 0.2	1.94 ± 0.02	0.050 ± 0.005	13.0[c]	20.7	−2.21
	Hf–O2	4.7 ± 0.5	2.14 ± 0.02	0.089 ± 0.009	2.5[d]	14	21.85
	Hf–C	2.9 ± 0.3	3.11 ± 0.03	0.112 ± 0.011		13	
	Hf–Hf	2.0 ± 0.4	3.42 ± 0.03	0.081 ± 0.008			
1 eq. HO^{i}Pr	Hf–O1	2.1 ± 0.2	1.94 ± 0.02	0.050 ± 0.005	13.0[c]	20.7	−2.21
	Hf–O2	5.0 ± 0.5	2.14 ± 0.02	0.089 ± 0.009	2.5[d]	14	23.71
	Hf–C	2.2 ± 0.2	3.13 ± 0.03	0.112 ± 0.011		13	
	Hf–Hf	1.7 ± 0.2	3.42 ± 0.03	0.081 ± 0.008			
2 eq. HO^{i}Pr	Hf–O1	1.8 ± 0.2	1.94 ± 0.02	0.045 ± 0.005	13.0[c]	20.7	−2.04
	Hf–O2	5.2 ± 0.5	2.14 ± 0.02	0.092 ± 0.009	2.5[d]	14	26.95
	Hf–C	2.2 ± 0.2	3.16 ± 0.03	0.112 ± 0.011		13	
	Hf–Hf	2.0 ± 0.2	3.42 ± 0.03	0.084 ± 0.008			
3 eq. HO^{i}Pr	Hf–O1	1.7 ± 0.2	1.93 ± 0.02	0.022 ± 0.002	13.0[c]	20.7	−1.77
	Hf–O2	5.4 ± 0.5	2.14 ± 0.02	0.095 ± 0.009	2.5[d]	14	30.92
	Hf–C	2.1 ± 0.2	3.16 ± 0.03	0.112 ± 0.011		13	
	Hf–Hf	1.8 ± 0.2	3.41 ± 0.03	0.087 ± 0.009			
1 eq. THF	Hf–O1	2.1 ± 0.2	1.94 ± 0.02	0.050 ± 0.005	13.0[c]	20.7	−1.59
	Hf–O2	4.9 ± 0.5	2.14 ± 0.02	0.089 ± 0.009	2.5[d]	14	22.08
	Hf–C	2.8 ± 0.3	3.10 ± 0.03	0.112 ± 0.011		13	
	Hf–Hf	2.1 ± 0.2	3.42 ± 0.03	0.084 ± 0.008			
3 eq. THF	Hf–O1	2.1 ± 0.2	1.94 ± 0.02	0.050 ± 0.005	13.0[c]	20.7	−1.46
	Hf–O2	5.0 ± 0.5	2.14 ± 0.02	0.089 ± 0.009	2.5[d]	14	23.98
	Hf–C	2.5 ± 0.3	3.10 ± 0.03	0.112 ± 0.011		13	
	Hf–Hf	2.0 ± 0.2	3.42 ± 0.03	0.084 ± 0.008			
1 eq. Hacac	Hf–O1	0.9 ± 0.1	1.94 ± 0.02	0.032 ± 0.003	13.0[c]	20.7	−2.69
	Hf–O2	6.3 ± 0.7	2.17 ± 0.02	0.077 ± 0.008	2.5[d]	14	15.48
	Hf–C	5.8 ± 0.6	3.19 ± 0.03	0.097 ± 0.010		13	
	Hf–Hf	1.5 ± 0.2	3.52 ± 0.04	0.067 ± 0.007			
2 eq. Hacac	Hf–O	7.6 ± 0.7	2.17 ± 0.02	0.084 ± 0.008	13.0[c]	12.4	−2.6719.3
	Hf–C	7.8 ± 0.8	3.21 ± 0.03	0.089 ± 0.009	1.5[e]	9	
						7	
3 eq. Hacac	Hf–O	8.3 ± 0.8	2.17 ± 0.02	0.084 ± 0.008	13.0[c]	12.4	−2.4119.3
	Hf–C	7.6 ± 0.8	3.20 ± 0.03	0.084 ± 0.009	1.5[e]	9	
						7	
Monoclinic HfO_2	Hf–O1	7[i]	2.12 ± 0.02	0.110 ± 0.011	13.0[c]	20.7	−1.54
	Hf–Hf1	7[i]	3.42 ± 0.03	0.097 ± 0.010	2.5[d]	14	32.03
	Hf–O2	7[i]	3.90 ± 0.04	0.110 ± 0.011		9	
	Hf–Hf2	4[i]	3.94 ± 0.04	0.107 ± 0.011			
$Hf_4O_2(OMc)_{12}$	Hf–O1	1.6 ± 0.2	2.06 ± 0.02	0.063 ± 0.006	13.0[c]	20.7	−2.6
	Hf–O2	5.9 ± 0.6	2.19 ± 0.02	0.092 ± 0.009	2.5[d]	14	26.58
	Hf–Hf	2.3 ± 0.2	3.48 ± 0.03	0.063 ± 0.006		10	

[a] Amplitude reducing factor (AFAC) = 0.8. [b] Abs = X-ray absorbing atom, Bs = backscatterer, R = distance, σ = Debye–Waller factor. [c] k_{min} = 3 Å^{-1}, k_{max} = 16 Å^{-1}. [d] R_{min} = 1.5 Å, R_{max} = 4.0 Å. [e] R_{min} = 2.0 Å, R_{max} = 3.5 Å. [f] Calculated according to $N_{ind} = 2\pi^{-1}(\Delta k \Delta R)$. [g] $N_{free} = 2/3N_{ind}$ [h] Quality of fit. [i] Coordination numbers were fixed to literature values.

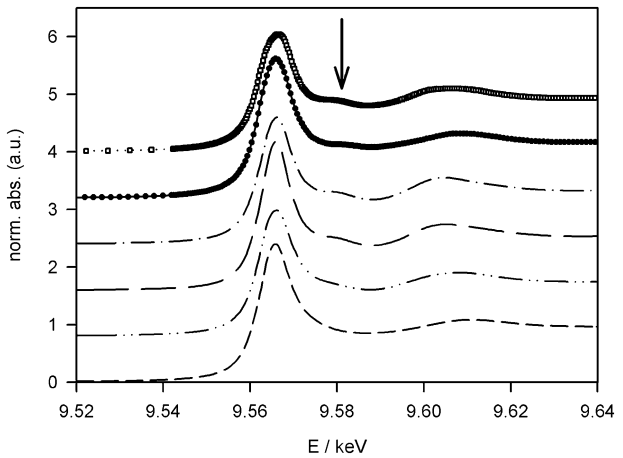

Fig. 2 XANES region of $Hf(OBu)_4$ (**1**) in toluene (**2**) (short dashed line), and after the addition of one (double dotted dashed line), two (long dashed line) and three (dotted dashed line) equivalents of Hacac, monoclinic HfO_2 (filled circles) and $Hf_4O_2(OMc)_{12}$ (open squares). The arrow marks the characteristic post-edge signal for seven- or eight-fold oxygen coordination.

Only two oyxgen shells can be fitted to the experimental data. The values are in accordance with the $Hf(O^iPr)_4(HO^iPr)$ (**3**) reference as determined by Veith *et al.*[11]

Hafnium compounds with oxygen coordination numbers of seven (HfO_2) or 7.5 (**6**) exhibit a signal in the XANES spectrum at around 9.58 keV.[33] Therefore, the absence of this signal in the spectrum of **1** in **2**, shown in Fig. 2, is indicative of an oxygen coordination smaller than seven, which is later confirmed in the EXAFS analysis.

The hafnium coordination number of two at a distance of 3.42 Å is contradictory to a dimeric structure in solution (*cf.* Scheme 1). A fit with a fixed Hf-coordination number of one, according to **I** resulted in a reduced quality of fit (*R*-factor) by more than 20%. Also, structure **III** deduced form $Hf_4O_2(OMc)_{12}$ (**6**) determined by Gross *et al.*,[21] can be excluded owing to the longer Hf–Hf distance. Although **1** in **2** and **6** show comparable hafnium coordination numbers, the higher intensity of the Hf-signal in the Fourier transform of **6** is explained by the smaller Debye–Waller factor. But both the experimental number of hafnium backscatterers and their distance are in good agreement with structure **II**, determined by Starikova *et al.* as subunit of $Hf_6O_2(OEt)_{20}(HOEt)_2$ (*cf.* Tables 1 and 4), or like in $Zr_3O(O^tBu)_{10}$.[29]

In solutions of metal alkoxides, formation of equilibria between different structure types can not be excluded *a priori*. Despite the fact that it might make the discussion not as straightforward as possible, we are convinced that in EXAFS investigations of complex solutions, it is mandatory to account for the inherent property of the method, namely to average over all species present, and to discuss the possible existence of different species. Simple mixtures that yield a Hf-coordination number of two are listed in Table 4 as M1 and M2. For simplicity, only well defined molar ratios are used for discussion. Nevertheless, this approximation does not affect the later results. While M1 still contains structure **II**, but in combination with **I** and **III** in a molar ratio of 2 : 1 : 1, M2 is only constructed by **I** and **III** in a 2 : 1 ratio. As M1 shows a distance more similar to the experiment than M2, M1 is more probable. There can also be more complicated mixtures than M1 and M2, that mirror the EXAFS results with the same quality. Two examples of such mixtures are listed in Table 2 as M3 and M4. Both illustrate the fact, that structure **II** is required to be the dominant one.

Even if the error in the coordination number is taken into account, like in the mixtures M5 to M8, the constructed mixtures can reproduce the experimentally obtained distance of the hafnium shell only, if the fraction of **II** becomes very high.

As a conclusion to this paragraph, the cyclic trimer **II** is identified to be the dominant structure. In contrast to $Zr(O^nBu)_4$, an increased degree of association is therefore observed for $Hf(O^nBu)_4$ in non-polar solvents, which is in accordance with ebullioscopic results by Bradley *et al.*[34] Surprisingly, in case of $Zr(O^nBu)_4$, such an increased aggregation could not be detected by EXAFS investigations.[10,20] The different cluster sizes of these two precursors in solution may be an explanation for their different reactivity in the synthesis of Hf- and Zr-oxo-alkoxide clusters.[21]

$Hf(O^nBu)_4$ in toluene with additional donor compounds

Fig. 1 also shows the experimental $\chi(k)$-spectra of **1** in **2** plus three equivalents HO^iPr or THF. The spectra for samples with one and two equivalents HO^iPr and one equivalent THF, respectively, were omitted for clarity.

From comparison of the spectra it can be seen that no changes take place, when the Lewis bases HO^iPr and THF are added. The iterations of *all* parameters gave stable results

Table 4 Average structural parameters for several mixtures of the reference compounds **I**, **II** and **III** used to describe the results obtained with EXAFS spectroscopy of $Hf(OBu)_4$ (**1**) in toluene (**2**)

Mixture[a]	I	II	III	Average hafnium coordination number[b]	Average hafnium distance [Å]
M1	2	1	1	1.8	3.52
M2	2	0	1	1.8	3.56
M3	2	2–∞	1	1.9	3.51–3.45
M4	1	10–∞	1	2.0	3.47–3.45
M5	5	1	1	1.5	3.51
M6	4	2	1	1.7	3.50
M7	2	2	2	2.0	3.53
M8	2	1	3	2.1	3.56

[a] Numbers of the complexes denote the unweighted molar ratios of the complexes (note: **I** contains two, **II** contains three and **III** contains four hafnium atoms). [b] Coordination numbers obtained in EXAFS spectroscopy, not identical with crystallographic coordination numbers.

identical to those of **1** in **2**. Only the carbon shells show slight variations, but the obtained Hf–C distances are similar to those obtained for related zirconium alkoxides.[35] The implementation of a carbon shell into the fitting procedure is necessary, as it improves the quality of fit by more than 40%. But it should be noted, that the properties of carbon as backscatterer at distances beyond the nearest neighbour shell restrict the reliability of the obtained coordination numbers.[36] Additionally, the carbon shell in alkoxides comprises Hf–C bonds of different ligands (terminal, bridging, alkoxide, alcohol) with similar distances. As the EXAFS signal of this shell is smeared out, the Debye–Waller factor is larger. Hence, these coordination numbers should only be used in a comparative way, with the value for pure **1** in **2** as standard.[20] The results of the EXAFS analyses are supported by the XANES region (see supplementary information, Fig. SF1†) where no changes could be observed when HO^{i}Pr or THF were added.

It can be stated that the local environment of the hafnium atoms remains unaltered, but we can not exclude an exchange of *n*-butoxide by *iso*-propanol and THF. This behaviour is similar to that of Zr(O^{n}Bu)$_4$, where also no changes were induced by these two ligands.

The XANES spectra of the solutions with one to three equivalents Hacac in Fig. 2 show an increasing intensity of the shoulder after the white line at 9.58 keV.

This is a first indication of an altered oxygen coordination, since the XANES region is dominated by multiple scattering effects in the nearest neighbour shells.[37] To support this interpretation the coordination properties of Hacac in solutions of **1** in **2** were studied by IR-spectroscopy. Fig. 3 shows the difference spectra between solutions with one to four equivalents Hacac and that of pure **1** in **2** in the region of 1500–1650 cm^{-1}. Two signals at around 1595 and 1530 cm^{-1} are assigned to the ν(C═C) and ν(C═O) stretching modes of the coordinated enolate ion, respectively.[38]

Both absorption bands show a linear increase of the integrated intensity up to three added equivalents Hacac (see also supplementary information, Table ST1 and Fig. SF2†). But with four Hacac the intensity at 1530 cm^{-1} remains unaltered.

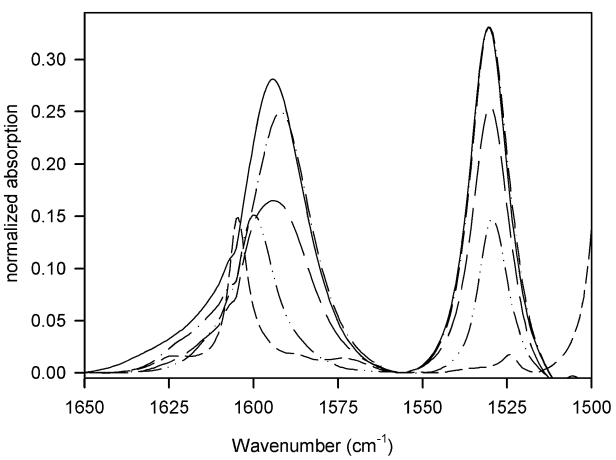

Fig. 3 C═O and C═C vibrational bands of the difference spectra between Hf(OBu)$_4$ (**1**) in toluene (**2**) (short dashed line), and with one (double dotted dashed line), two (long dashed line), three (dotted dashed line) and four (solid line) equivalents Hacac.

The slight deviation of the band at 1595 cm^{-1} from this behaviour can be explained by the fact that solvent signals interfere with this signal (see supplementary information, Fig. SF3†). Together with the fact that characteristic signals of free Hacac[39] between 1700 and 1730 cm^{-1} are only observed with four equivalents Hacac (see supplementary information, Fig. SF4†) it can be concluded, that in the solutions of **1** in **2** *all* Hacac ligand molecules present in solution coordinate up to a maximum of three equivalents per hafnium center, and no free Hacac remains until the concentration of Hacac exceeds three equivalents. This result forms the frame for the following discussion of the EXAFS results.

The increased average coordination number of the oxygen shell after the addition of Hacac (*cf.* Table 3) can be qualitatively explained by a progressing exchange of monodentate [O^{n}Bu]$^-$ against bidentate [acac]$^-$, which also causes a change in the Hf–C distance in accordance with the literature.[40] Also, the higher coordination number in the carbon shell can be explained by this exchange, since [O^{n}Bu]$^-$ ligands provide one carbon neighbour, while [acac]$^-$ provides at least two carbon atoms per ligand. But as already mentioned, no exact quantitative discussion of the carbon shell is possible.[36] All these effects are also clearly visible in the Fourier transforms of the experimental $\chi(k)$-functions, shown in Fig. 4, where the signals of the second oxygen and the carbon shell continuously increase, while the first O- and the Hf-peak vanish with increasing Hacac concentration.

Although the oxygen coordination number found with one equivalent Hacac would be in accordance with structure **IV** or **V**, the number of 1.5 hafnium neighbours is contradictory to such a simple situation according to the following reactions (1) or (2):

$$\mathbf{II} + 3\ \text{Hacac} \rightarrow \mathbf{IV} + 3\ ^n\text{BuOH} \quad (1)$$

$$2\ \mathbf{II} + 6\ \text{Hacac} \rightarrow 3\ \mathbf{V} + 6\ ^n\text{BuOH} \quad (2)$$

$$4\ \mathbf{II} + 12\ \text{Hacac} \rightarrow 2\ \mathbf{IV} + 3\ \mathbf{V} + 12\ ^n\text{BuOH} \quad (3)$$

$$4\ \mathbf{II} + 12\ \text{Hacac} \rightarrow 2\ \mathbf{II} + 3\ \mathbf{VII} + 12\ ^n\text{BuOH} \quad (4)$$

$$8\ \mathbf{II} + 24\ \text{Hacac} \rightarrow 2\ \mathbf{II} + 2\ \mathbf{IV} + 3\ \mathbf{V} + 3\ \mathbf{VII} + 12\ ^n\text{BuOH} \quad (5)$$

A detailed discussion of possible reactions, involving the structures of Scheme 1, gives three reactions (3)–(5), that reproduce the obtained experimental values to a largest extent (see supplementary information, Scheme SS1 and Table ST2†). In contrast to the discussed solid state structures of diketone-substituted Hf- and Zr-alkoxides,[14d,29] our EXAFS results demand the coordination of a neutral ^{n}BuOH ligand to achieve the obtained sevenfold Hf–O coordination with one equivalent Hacac. While (3) is in accordance with solid mono-substituted Zr$_2$(O^{n}Pr)$_6$(tmhd)$_2$, Zr$_2$(O^{i}Pr)$_6$(acac)$_2$ and Hf$_2$(O^{n}Pr)$_6$(tmhd)$_2$ (**8**), the reactions (4) and (5) can provide an explanation for the changes, when these solid compounds are dissolved.[14d,41] But in contrast to Kessler *et al.*,[14d] who suggest rearrangement of Hf$_2$(O^{n}Pr)$_6$(tmhd)$_2$ mainly to tetra-substituted Hf(tmhd)$_4$ and dimeric hafnium *n*-propoxide, in our study the complex **II** and the di-substituted dimer **VII** are the only possible species, existing in solution, that are in accordance with the EXAFS results. The analog to structure

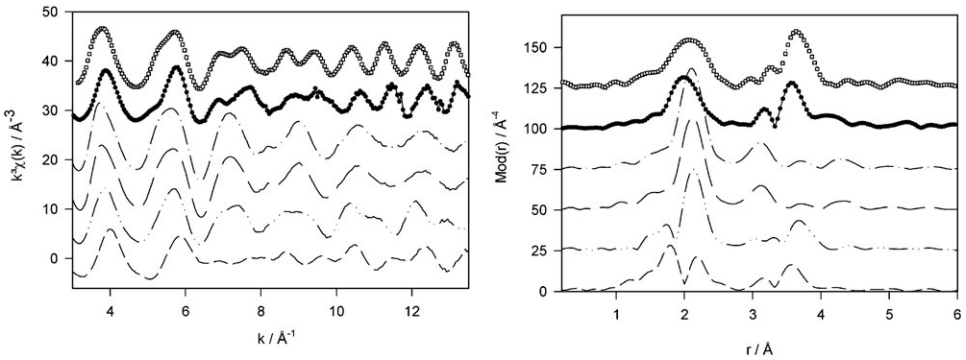

Fig. 4 Experimental $k^3 \cdot \chi(k)$ functions (left) of **1** in **2** (short dashed line), as well as containing one (double dotted dashed line), two (long dashed line) and three (dotted dashed line) equivalents of Hacac, monoclinic HfO_2 (filled circles) and $Hf_4O_2(OMc)_{12}$ (open squares), together with their Fourier transforms (right).

VII, $Ce_2(O^iPr)_4(acac)_4$ had already been found for the modification of $Ce(O^iPr)_3$ with Hacac by means of EXAFS spectroscopy.[17,42,43] The only dimeric di-substituted Hf–alkoxide is complex **9**. Three-substituted structures like **VIII** can therefore be ruled out in solutions of $Hf(O^nBu)_4$ with one equivalent Hacac in toluene. Therefore a similar behaviour of $Hf(O^nBu)_4$ to that found by Kessler *et al.* in analogy to reaction (2) by means of NMR spectroscopy[41] for $Zr(O^iPr)_4$ with one equivalent Hacac can not be confirmed by EXAFS spectroscopy.

Despite the fact that the limits of EXAFS spectroscopy are reached at this stage, and no definite decision for one of the reactions (3)–(5) can be made due to their identical coordination numbers, it can be concluded that the aggregation degree of the original complex formed by **1** in **2** is reduced when one mole equivalent Hacac is added.

With two equivalents Hacac further reduction of the aggregates solely to monomers can be observed, since no Hf–Hf shell can any longer be adjusted to the experimental data. Therefore, the mechanism proposed in ref. 41 for the reaction of mixed ligand zirconium-propoxides with two equivalents Hacac can not be applied here. Instead of a mixture of tri- and tetra-substituted monomers and the unsubstituted dimer, only the monomeric disubstituted complex **VI** in accordance with Jones *et al.*[44] is possible from our EXAFS analysis:

$$\mathbf{II} + 6\ \text{Hacac} \rightarrow 3\ \mathbf{VI} + 6\ {}^n\text{BuOH} \qquad (6)$$

The obtained Hf–O coordination number of 7.8 in a single shell (no second shell could be fitted) can only be explained by the coordination of a second neutral ^{n}BuOH ligand. In ref. 19 it was shown for aqueous hafnium solutions, that an eightfold oxygen coordination by ionic and neutral ligands results in a single O-shell with a distance of 2.15 Å.

With three equivalents of Hacac, only the monomer complex **VIII** can be deduced from the EXAFS results, since no Hf–Hf neighbours are found again. By consideration of the IR-spectroscopic results it can be concluded that the eightfold oxygen coordination in **VIII** is achieved by three $[acac]^-$, one $[O^nBu]^-$ and one ^{n}BuOH ligands. Although in principle a mixture of monomeric **VI** and $Hf(acac)_4$ would yield an oxygen coordination number of the same order, this combination is unlikely, since even no formation of $Hf(acac)_4$ could be detected by IR-spectroscopy. The same behaviour was found in our previous studies for $Zr(O^nBu)_4$.[20]

Correlation of the XANES signal at 9.58 keV to the oxygen coordination number

The XANES regions of the samples, shown in Fig. 2, contain a signal at around 9.58 keV. Obviously the intensity of this signal varies for the different samples. Isolation of this particular signal was carried out according to the procedure, described in the experimental section. As an example the deconvoluted XANES spectrum of the solid reference $Hf_4O_2(OMc)_{12}$ (**6**) is shown in Fig. 5.

Details of the obtained spectral parameters for all samples are given in the supplementary information (Table ST3†). As it can be seen in Fig. 6, the height of the isolated signal at ~9.58 keV exhibits a linear correlation to the experimentally determined average oxygen coordination number.

Although the integral intensity shows a similar trend, the peak height is preferable, due to the better correlation factor of $R = 0.966$ in comparison to $R = 0.939$ for the integrated

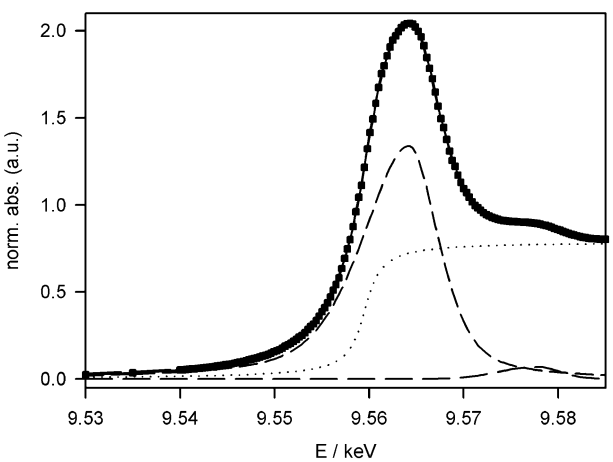

Fig. 5 Example of a deconvoluted XANES spectrum of $Hf_4O_2(OMc)_{12}$. The edge step is approximated by an arctan function (dotted line), the white line by a asymmetric Psoido-Voigt (short dashed line) and the signal at around 9.58 keV by a asymmetric Gaussion (long dashed line) function. The addition of all three parts (solid line) fits the experimental XANES spectrum (solid squares) very well.

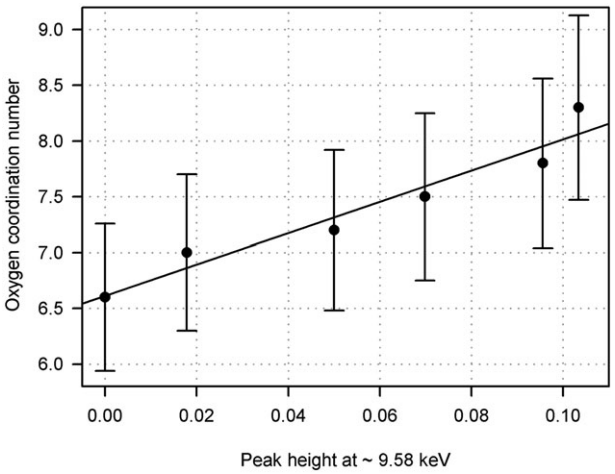

Fig. 6 Correlation of the signal intensity of the XANES signal after the white line at ~9.58 keV and the oxygen coordination number obtained for different samples discussed in the text. The analytical form of the regression function is $N(O) = 14.03(\pm 1.87) \cdot PPH + 6.61(\pm 0.13)$, where PPH is the signal height and N(O) the oxygen coordination number. The correlation factor is $R = 0.966$.

intensity. This empirical correlation can be used as indicator or measure for the average oxygen coordination number, regardless of the exact coordination geometry. It is the first time that such a model-independent interpretation of this feature of hafnium XANES spectra has been given.

Conclusions and outlook

With this work we showed the potential of X-ray absorption spectroscopy (XAS) as an experimental method to identify structures formed by alkoxide precursors in solution, for hafnium *n*-butoxide as examples. In comparison to standard analytical methods, EXAFS spectroscopy probes the clusters size directly by "counting" the metal neighbours around an X-ray absorbing atom. But on the other hand, XAS has the disadvantage of averaging over all species present in the solutions. Therefore first we determined the coordination numbers with high reliability by the use of different *k*-weightings. In a second step we compared our results with the structures of well-known solid state references of defined geometry, that form the basis for the discussion of possible mixtures of different species, and combined the results with a second spectroscopic method. This approach allowed the identification of a cyclic trimer as the main component in solutions of $Hf(O^nBu)_4$ in toluene. While HO^iPr and THF do not alter the hafnium framework, one equivalent of Hacac causes partial degradation to a disubstituted dimeric structure. With two and three Hacac, only di- and tri-substituted monomers are formed.

The evaluation of the XANES signal at around 9.58 keV can be used in future studies of such systems as a first measure of the average oxygen coordination number in addition to the EXAFS analysis. The obtained structural parameters can be used as input for first-principle multiple scattering calculations to obtain a deeper insight into the geometrical details of the clusters. Such calculations will be carried out for the present system, to achieve also a theoretical explanation for the empirical XANES-oxygen coordination relation.

Acknowledgements

We thank HASYLAB at DESY for provision of synchrotron radiation facilities and the staff of the beamline A1 for their support.

References

1 C. J. Brinker and G. W. Scherer, *Sol–Gel Science: The Physics and Chemistry of Sol–Gel Processing*, Academic Press, Boston, 1990.
2 C. A. C. Sequeira and M. J. Hudson, *Multifunctional Mesoporous Inorganic Solids*, Kluwer Academic Publishers, Boston, 1993.
3 (*a*) P. A. Williams, J. L. Roberts, A. C. Jones, P. R. Chalker, N. L. Tobin, J. F. Bickley, H. O. Davies, L. M. Smith and T. J. Leedham, *Chem. Vap. Deposition*, 2002, **8**, 163; (*b*) A. C. Jones, *J. Mater. Chem.*, 2002, **12**, 2576; (*c*) P. A. Williams, J. L. Roberts, A. C. Jones, P. R. Chalker, J. F. Bickley, A. Steiner, H. O. Davies and T. J. Leedham, *J. Mater. Chem.*, 2002, **12**, 165.
4 L. C. Klein, *Sol–Gel Technology for thin Films, Fibres, Preforms, Electronics and speciality Shapes*, Academic Press, Boston, 1988.
5 C. J. Brinker, D. E. Clark and D. R. Ulrich, *Better Ceramics through Chemistry I*, Elsevier Science Publishers, New York, 1984, vol. 32.
6 L. Armelao, H. Bertagnolli, S. Gross, V. Krishnan, U. Lavrencic-Stangar, K. Müller, B. Orel, G. Srinivasan, E. Tondello and A. Zattin, *J. Mater. Chem.*, 2005, **15**, 1954.
7 G. Kickelbick, M. P. Feth, H. Bertagnolli, M. Puchberger, D. Holzinger and S. Gross, *J. Chem. Soc., Dalton Trans.*, 2002, 3892.
8 (*a*) D. C. Bradley, R. C. Mehrotra and D. P. Gaur, *Metal Alkoxides*, Academic Press, London, 1978; (*b*) D. C. Bradley and C. E. Holloway, *Inorg. Chem.*, 1964, **3**, 1163.
9 L. G. Pfalzgraf, *New J. Chem.*, 1987, **11**, 663.
10 (*a*) D. Peter, T. S. Ertel and H. Bertagnolli, *J. Sol-Gel Sci. Technol.*, 1994, **3**, 91; (*b*) D. Peter, T. S. Ertel and H. Bertagnolli, *J. Sol-Gel Sci. Technol.*, 1995, **5**, 5.
11 M. Veith, S. Mathur, C. Mathur and V. Huch, *J. Chem. Soc., Dalton Trans.*, 1997, 2101.
12 V. W. Day, W. G. Klemperer and M. M. Pafford, *Inorg. Chem.*, 2001, **40**, 5738.
13 B. A. Vaartstra, J. C. Huffmann, P. S. Gradeff, K. Yunhu, L. G. Huber-Pfalzgraf, J. D. Dara, S. Paraud and K. G. Caulton, *Inorg. Chem.*, 1990, **29**, 3126.
14 (*a*) R. C. Mehrotra, J. M. Batwara and P. N. Kapoor, *Coord. Chem. Rev.*, 1980, **31**, 67; (*b*) M. Gugliemi and G. Carturan, *J. Non-Cryst. Solids*, 1988, **100**, 16; (*c*) J. Livage, M. Henry and C. Sanchez, *Prog. Solid State Chem.*, 1988, **18**, 259; (*d*) G. I. Spijksma, H. J. M. Bouwmeester, D. H. A. Blank, A. Fischer, M. Henry and V. G. Kessler, *Inorg. Chem.*, 2006, **45**, 4938.
15 (*a*) C. Sanchez, F. Babonneau, S. Doeuff and A. Leaustic, *Ultrastructure Processing of Advanced Ceramics*, J. Wiley & Sons, New York, 1988; (*b*) F. Babonneau, S. Doeuff, A. Leaustic, C. Sanchez, C. Cartier and M. Verdaguer, *Inorg. Chem.*, 1988, **27**, 3166.
16 U. Reinöhl, H. Bertagnolli, T. S. Ertel, W. Hörner and A. Weber, *Ber. Bunsen-Ges. Phys. Chem.*, 1998, **102**, 144.
17 F. Ribot, P. Toledano and C. Sanchez, *Chem. Mater.*, 1991, **3**, 759.
18 C. Hagfeldt, V. Kessler and I. Persson, *Dalton Trans.*, 2004, 2142.
19 A. L. Hector and W. Levason, *Eur. J. Inorg. Chem.*, 2005, 3365.
20 M. Bauer, C. Gastl, C. Köppl, G. Kickelbick and H. Bertagnolli, *Monatsh. Chem.*, 2006, **137**, 567.
21 S. Gross, G. Kickelbick, M. Puchberger and U. Schubert, *Monatsh. Chem.*, 2003, **134**, 1053.
22 T. S. Ertel and H. Bertagnolli, *Nucl. Instrum. Methods Phys. Res., Sect. B*, 1995, **73**, 199.
23 (*a*) T. S. Ertel, H. Bertagnolli, S. Hückmann, U. Kolb and D. Peter, *Appl. Spectrosc.*, 1992, **46**, 690; (*b*) M. Newville, P. Livins, Y. Yacoby, J. J. Rehr and E. A. Stern, *Phys. Rev. B: Condens. Matter*, 1993, **47**, 14126.

24 (*a*) N. Binsted and S. S. Hasnain, *J. Synchrotron. Radiat.*, 1996, **3**, 185; (*b*) N. Binsted and F. Mosselmans, *EXCURV98 Manual*, Daresbury, UK.
25 S. I. Zabinsky, J. J. Rehr, A. Ankudinov, R. C. Albers and M. J. Eller, *Phys. Rev. B*, 1995, **52**, 2995.
26 D. C. Koningsberger, B. L. Mojet, G. E. van Dorssen and D. E. Ramaker, *Top. Catal.*, 2000, **10**, 143.
27 T. Ressler, *J. Phys. IV*, 1997, **C2–7**, 269.
28 B. A. Vaartstra, J. C. Huffmann, P. S. Gradeff, K. Yunhu, L. G. Hubert-Pfalzgraf, J. D. Dara, S. Paraud and K. G. Caulton, *Inorg. Chem.*, 1990, **29**, 3126.
29 Z. A. Starikova, E. P. Turevskaya, N. I. Kozlova, N. Ya. Turova, D. V. Berdyev and A. I. Yanovsky, *Polyhedron*, 1999, **18**, 941.
30 K. A. Fleeting, P. O'Brian, D. J. Otway, A. J. P. White, D. J. Williams and A. C. Jones, *Inorg. Chem.*, 1999, **38**, 1432.
31 (*a*) B. Allard, *J. Inorg. Nucl. Chem.*, 1976, **38**, 2109; (*b*) S. V. Pasko, L. G. Hubert-Pfalzgraf, A. Abrutis, P. Richard, A. Bartasyte and V. Kazlauskiene, *J. Mater. Chem.*, 2004, **14**, 1245.
32 R. E. Hahn, P. R. Suitch and J. L. Pentecost, *J. Am. Ceram. Soc.*, 1985, **68**, 285.
33 R. E. Hann, P. R. Suitch and J. L. Pentecost, *J. Am. Ceram. Soc.*, 1985, **68**, 285.
34 D. C. Bradley and C. E. Holloway, *Inorg. Chem.*, 1964, **3**, 1163.
35 V. W. Day, W. G. Klemperer and M. M. Pafford, *Inorg. Chem.*, 2001, **40**, 5738.
36 Due to the small scattering amplitude of the light backscatterer carbon, the relatively larger distance of the carbon shell, which causes high frequency oscillations of weak intensity in the EXAFS signal, and the limited mean free path, the extraction of the carbon contribution from the total EXAFS signal shows an inherent uncertainty.
37 F. Farges, G. E. Brown and J. J. Rehr, *Phys. Rev. B*, 1997, **56**, 1809.
38 (*a*) K. Nakamoto, *Infrared and Raman Spectra of Inorganic and Coordination Compounds*, John Wiley & Sons, New York, 1986; (*b*) Neither of the vibrations at 1595 and 1530 cm^{-1} are the pure ν(C═C) and ν(C═O) modes, but combinations of ν(C═C) + ν(C═O) and ν(C═O) + ν(C═C), respectively. This detail has been omitted for clarity in the discussion.
39 K. L. Wierzchowski and D. Shugar, *Spectrochim. Cosmochim. Acta*, 1965, **21**, 943.
40 S. V. Pasko, L. G. Hubert-Pfalzgraf, A. Abrutis, P. Richard, A. Bartasyte and V. Kazlauskiene, *J. Mater. Chem.*, 2004, **14**, 1245.
41 G. I. Spijksma, H. J. M. Bouwmeester, D. H. A. Blank and V. G. Kessler, *Chem. Commun.*, 2004, 1874.
42 P. Toledano, F. Ribot and C. Sanchez, *C. R. Acad. Sci., Ser. II*, 1990, **311**, 1315.
43 C. Sanchez, P. Toledano and F. Ribot, *Better Ceramics Through Chemsitry IV*, MRS, Pittsburgh, 1990, p. 47.
44 A. C. Jones, T. J. Leedham, P. J. Wright, M. J. Crosbie, P. A. Lane, D. J. Williams, K. A. Fleeting, D. J. Ottway and P. O'Brian, *Chem. Vap. Deposition*, 1998, **4**, 46.